Available online at www.sciencedirect.com
SCIENCE DIRECT®
C. R. Physique 6 (2005) 451–466
COMPTES RENDUS PHYSIQUE
http://france.elsevier.com/direct/COMREN/

Aircraft trailing vortices/Tourbillons de sillages d'avions

Predicting the near-field evolution of airplane trailing vortices

Michael Czech [a], Gregory Miller [a], Jeffrey Crouch [a,*], Michail Strelets [b]

[a] *Boeing Commercial Airplanes, Seattle, USA*
[b] *Federal Scientific Center 'Applied Chemistry', St Petersburg, Russia*

Available online 5 July 2005

Abstract

The near-field (up to about 20 spans) development of trailing vortices is investigated experimentally and numerically. Computational Fluid Dynamics (CFD) results are based on the solution of quasi-3D Reynolds-averaged Navier–Stokes equations with a one-equation turbulence model. The inclusion of turbulence effects is found to be essential to capturing the correct near-field development. The CFD results are shown to be in very good agreement with experimental wake-survey results out to ten spans. Results show that wing loadings typical of commercial airplanes in a landing configuration can lead to multiple, or single vortex pairs, at distances of fifteen to twenty spans downstream. ***To cite this article: M. Czech et al., C. R. Physique 6 (2005).***

Résumé

Prédiction de l'évolution des tourbillons de sillage d'avions dans le champ proche. Le développement d'un sillage tourbillonnaire dans le champ proche d'un avion (jusqu'à 20 envergures) est étudié expérimentalement et numériquement. L'approche numérique est basée sur la résolution des équations de Navier–Stokes moyennées au sens de Reynolds, auxquelles on adjoint un modèle de turbulence à une équation de transport. On montre ainsi que les effets de turbulence jouent un rôle primordial sur la dynamique du sillage dans le champ proche. Les résultats numériques sont en très bon accord avec les résultats expérimentaux, jusqu'à environ 10 envergures. Les résultats montrent que les lois de charge typiques d'un avion commercial en configuration d'atterrissage peuvent aboutir, à des distances de quinze à vingt envergures, à des configurations tourbillonnaires très diverses, comportant un seul ou plusieurs dipôles. ***Pour citer cet article : M. Czech et al., C. R. Physique 6 (2005).***

Keywords: CFD; RANS; Turbulence; Vortices; Vortex merger; Wake survey

Mots-clés : CFD ; RANS ; Turbulence ; Tourbillons ; Fusion de tourbillons ; Mesures

1. Introduction

Recent efforts to break up airplane trailing vortices have exploited a system of multiple vortex pairs that is produced by airplanes with flaps deployed [1–5]. This system of vortices admits new instabilities, which are faster growing than the instabilities on a single pair of vortices. The instabilities, and the associated breakup schemes, are linked to specific features of the multiple vortex-pair system (e.g., a co-rotating pair, or a counter-rotating pair, on each side of the airplane). Therefore, the design and

* Corresponding author.
E-mail address: jeffrey.d.crouch@boeing.com (J. Crouch).

1631-0705/$ – see front matter
doi:10.1016/j.crhy.2005.05.005

assessment of any of these vortex-breakup schemes require detailed information about the near-field evolution of the trailing vortices up to twenty or thirty spans downstream.

The initial vortex system can be determined using a wake survey at the tail of the airplane, measured in a wind tunnel at moderate Reynolds numbers. This provides the initial vorticity distribution and the axial (streamwise) velocity. However, this may not provide any insight into the multiple vortex system that exists ten or twenty spans downstream due to the complicated vortex evolution in the near field. In some cases, the vortices may rapidly merge into a single vortex on each side of the airplane. In other cases, two or three vortex pairs may persist out to twenty or thirty spans downstream. How the wake evolves depends on the details of the initial vorticity distribution, atmospheric conditions, the level of turbulent mixing across the center plane, and the rate at which the vortices merge. Engine thrust effects will also play a role, but this has generally been neglected except in flight testing.

Obtaining quantitative information about trailing vortices behind realistic configurations at downstream distances as far as twenty spans is difficult. Wind tunnels that are large enough to achieve such distances behind conventional high-lift models are relatively scarce. Models that are small enough to achieve such distances in a conventional wind tunnel face the challenge of performing at low Reynolds numbers. Also, these models may not simulate the flow field behind a full-scale airplane with a fidelity that is comparable to a conventional model, like one used for aerodynamic development.

In earlier studies, Fell and Staufenbiel [6] measured flap and tip vortices up to six spans downstream, and de Bruin, Hegen, Rohne and Spalart [7] measured flap and tip vortices up to five spans downstream. A follow on to the study of de Bruin et al. measured thirteen spans downstream by placing the model in the large DNW wind tunnel. More recently, Jacquin, Fabre, Geffroy and Coustols [8] made very detailed measurements in the wake of a flapped-wing configuration up to nine spans downstream using a half model. Bellastrada, Breitsamter and Laschka [9] experimentally investigated vortices shed from an aircraft half-model in a high-lift configuration. A triple hot-wire probe was used to acquire both mean and unsteady flow at several transverse planes up to 5.6 wing spans downstream of the tail.

An alternative is to use the wind tunnel wake survey to develop a model that can be operated in a water towing-tank facility. Jacob and Savaş [10] used the combination of wind tunnel and towing tank to study the near- and far-field development of flapped wings. They used PIV in the towing tank to obtain quantitative information about the merger of flap and tip vortices. A similar approach was used by Stuff [11] and by Durston et al. [12] to study the interaction of wing-tip vortices and tail vortices. The work of Crouch, Miller and Spalart [5] used a conventional wind-tunnel model to calibrate a towing-tank model in the wind tunnel—and then examined the evolution of the vortices in the towing tank from the tail of the airplane out to the far field using dye flow visualization. This approach enabled a realistic airplane-configuration wake to be studied into the far field. Another approach that enables a study of the vortices far downstream is to catapult the model through the air. Coustols et al. [13] have used this approach to follow the vortices up to seventy spans downstream.

The primary shortcoming of these various experimental approaches is that they are costly and time consuming. This is particularly the case if information is needed beyond, say, ten spans downstream. A more practical means to assess realistic airplane configurations is to make use of computational fluid dynamics (CFD) to evolve the near-field wake. This assumes, however, that the CFD is able to capture the essential details of the near-field evolution. The CFD also provides the potential for incorporating engine thrust effects.

Many of the earlier CFD studies of the near-field wake have treated the vortices as laminar (e.g., de Bruin et al. [7]) or as inviscid (e.g., Benkenida et al. [14], Stumpf [15]). This provides a good approximation when there are distinct vortices, but it does not adequately capture vortex merger or vortex cancellation on the center plane. Shur et al. [16] solved the Reynolds-Averaged Navier–Stokes (RANS) equations with a turbulence model. They made comparisons to the experiments of de Bruin et al. up to thirteen spans downstream. They considered a few different turbulence models, and found that the SA model [17] with rotation and curvature corrections [18] provided the best overall agreement with the experiments. Although vortex merger was seen to occur too late, trajectories of the tip and flap vortices were found to agree generally well with experimental data from de Bruin et al. Limitations in the empirical initialization of the eddy viscosity and domain size might have led to some differences observed between the numerical predictions and experimental observations.

To use the CFD results to predict the features important for controlling the vortex breakup, the CFD must be able to predict the vortex merger and to capture the demise of vortices on the center plane. In this paper we consider the near-field evolution of the trailing vortices in an effort to determine which airplane configurations are amenable to trailing vortex control. We present experimental and numerical results for the development of the vortices behind realistic flaps-down airplane configurations. Wind-tunnel wake surveys measured at the tail of the airplane are used to initiate the CFD calculations. Using a relatively small model in a large wind tunnel, wake surveys were taken as far downstream as ten spans. The downstream measurements are used to help delineate boundaries of good, or bad, configurations and to help validate the CFD methodology. The CFD is then used to estimate key trailing-vortex parameters based on the tail-plane wake surveys. These parameters include circulation ratios and the nondimensional separation distance between the flap and tip vortices δ_{yz}. Thrust effects are not considered in the presented results. However, the inclusion of these effects is discussed in the conclusions.

2. Description of methods

2.1. Wind tunnel surveys and towing-tank visualizations

Wake survey data was measured behind a small model in a large wind tunnel using the technique of Crowder, Watzlavick and Krutckoff [19]. The model, as shown in Fig. 1, has an unswept wing and a tail attached to a fuselage. It is capable of producing a wide variety of different wake flow fields by means of relatively simple changes to the wing trailing-edge sections or the tail. These included inboard- and outboard-flap spans, tail span, and section lift coefficients. The position and strength of vorticity trailing from the tip, the inboard flap and the tail were the principal variables in the present study. However, the available configurations encompassed a range of realistic airplane configurations. In each of the examples used here, wing lift and tail download coefficients approximated those of an airplane on approach to landing. This was demonstrated by comparing the measurements to wake-survey data from behind a larger conventional high-lift model. A wing span of 0.91 m and a relatively low chord Reynolds number of 600 000 were selected because of other design requirements (e.g., using this model in a water towing tank to study the far wake), but the small size allowed wake surveys up to 10 wing spans downstream in the wind tunnel.

Two series of wake surveys were conducted. The first series were measured at the 14 × 22 Wind Tunnel at NASA Langley Research Center. The tunnel cross section measures 4.27 m high by 6.71 m wide, and the length of the test section allowed surveys at up to 9.45 m downstream of the model—before the divergent diffuser section. The second series of surveys were measured at the Boeing V/STOL Wind Tunnel (BVWT), with a cross section of 6.10 m × 6.10 m and the length allowed measurements up to 3.66 m downstream of the tail. The free-stream velocity was 60 m/s in both tests.

The wake survey technique, described in [19], employed a single conical 5-hole probe scanned in a plane normal to the free-stream direction, using a two-rotary axis device that moved through a succession of arcs. The distance between sample points is about 0.3% or 0.7% of the model wing span, and the probe traversing rates are 0.4% or 1% of free-stream velocity. This provided adequate resolution and accuracy, so those were typical values used during the test. Following the acquisition of a complete survey, the velocity, the static pressure and the total pressure were interpolated onto a rectangular grid of the same spacing, where vorticity could then be more easily calculated. The first transverse survey station is nominally 3.8 cm behind the tail and this location is referred to as $x = 0$.

Flow visualization experiments were conducted in the U.S. Navy David Taylor Model Basin shallow water basin which is 350 m long, 15.5 m wide and 6.7 m deep. The model was essentially the same as used in the wind tunnel surveys and positioned 1.80 m below the water surface. The trailing vortices were visualized using fluorescent dye injected at the outer edge of the inboard flap, the outer edge of the outboard flap, the wing tip and the horizontal tail. Time-coded video cameras were placed at various positions to monitor the positions of the vortices. A laser light sheet provided an end-view of the vortices and from this the vortex core positions were estimated.

2.2. CFD approach

The CFD approach is based on the solution of the Reynolds-Averaged Navier–Stokes (RANS) equations using the SA turbulence model [17] with rotation and curvature corrections [18] (referred to as the SARC model). This turbulence model was

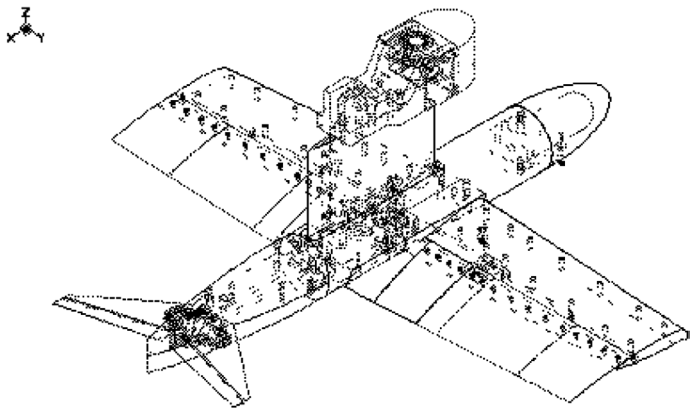

Fig. 1. Generic airplane model used in wind tunnel surveys (0.91 m wingspan, $Re = 600\,000$).

shown to perform well for trailing-vortex flows in terms of numerical efficiency and the relative agreement with experimental results [16]. A Cartesian coordinate system is employed where the x coordinate is along the flight path, y is in the span direction and z is in the vertical direction. All coordinates are normalized by the geometric wing span b, and the velocities are normalized by the free-stream value U_∞. This gives a Reynolds number of $Re = U_\infty b/\nu = 3.6 \times 10^6$.

The fully three-dimensional steady RANS equations are approximated by a quasi-3D formulation. This assumes that the streamwise derivatives in the 3D RANS equations are negligible, except for those in the convective terms (e.g., terms of the type $u(\partial f/\partial x)$). The convective terms are simplified by replacing the local streamwise velocity, u, by its free-stream value U_∞ (i.e., $u(\partial f/\partial x) \approx U_\infty(\partial f/\partial x)$). This assumption does not imply a constant streamwise velocity, since the model retains the u-momentum equation, and therefore accounts for the transverse velocity gradients $\partial u/\partial y$ and $\partial u/\partial z$. These gradients contribute to the vorticity, and more significantly, to the generation of turbulence in the wake. This RANS approach cannot capture instabilities so the results focus on the mean evolution.

Numerically, the quasi-3D formulation is implemented as an unsteady 2D RANS calculation. The time variable corresponds to the 'marching coordinate' x/U_∞. However, unlike an unsteady 2D calculation, the system includes an additional transport equation for the u-velocity component. The system is numerically integrated using the time-accurate implicit upwind flux-difference scheme of Rogers and Kwak [20]. The inviscid fluxes are approximated with third-order accuracy and the 'time' (marching coordinate) derivatives with second-order accuracy. At each time step the finite difference equations are solved iteratively using Gauss–Seidel relaxation for the continuity and momentum equations, and with the Diagonally-Dominant ADI algorithm for the eddy-viscosity transport equation. This quasi-3D approach is much cheaper than numerically solving the full 3D RANS equations. Comparisons between the quasi-3D and the full 3D solutions showed good agreement for a closely-related problem of a vortical wake behind a high-lift wing [16].

The boundary conditions chosen are slip walls. Detailed domain and grid variations were carried out to assess their impact on mid-field parameters. This lead to the selection of a standard grid of about 60 000 points in the half domain, shown in Fig. 2. The left plot shows the overall domain size and the grid, where only every 10th point is plotted for clarity. The right plot is zoomed in near the tail illustrating the resolution in this region with all points plotted. The tail vortex is covered by about 30 grid points in y and 10 points in z at $x/b = 0.0$. The half domain size is typically 2.0 spans in the spanwise direction, y, and 3.9 spans in the vertical direction, z. The relatively small domain leads to a predictable reduction in the mean decent rate, but does not significantly impact the vortex interactions.

A 'preprocessor' reads in the experimental data and interpolates them onto the computational grid. The interpolated streamwise velocity is directly used as the inflow boundary condition (outside the experimental window it is assumed to equal U_∞). For the transverse velocity components, the data is smoothed by solving the Poisson equation for the stream function associated with the experimental vorticity field (outside the experimental window the vorticity is assumed to be zero).

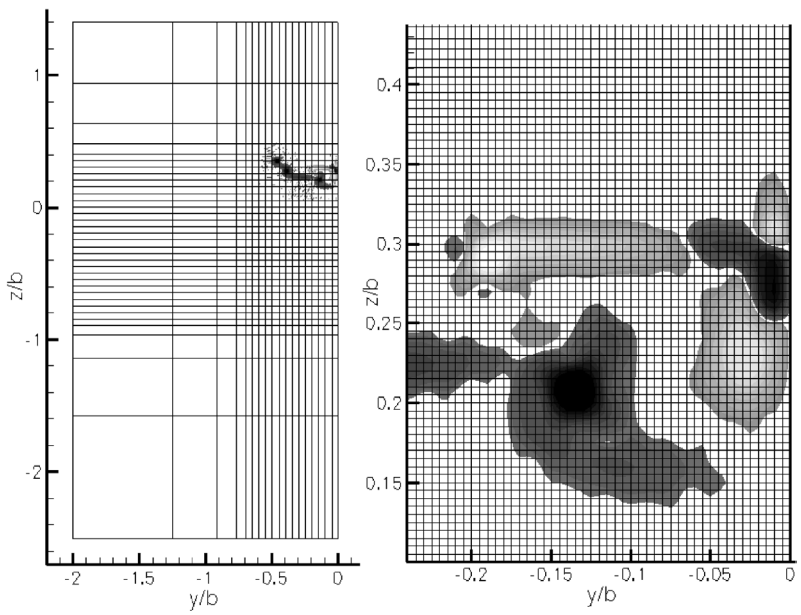

Fig. 2. Computational domain and grid (every 10th grid point shown in left-hand plot).

2.3. Eddy-viscosity initialization

The RANS calculation also requires an initialization of the eddy-viscosity field. A simple algebraic model is used to compute this field from a mixing length, based on the streamwise velocity component. The strain S is first computed from the streamwise velocity derivatives for the entire flow field. For typical airplane configurations the streamwise velocity variations are dominated by the fuselage wake (from the body boundary layer). Therefore, the level of the initial eddy viscosity field is set based on the fuselage wake which is approximated by an annular shear layer. For a better statistical estimate, the strain values are averaged over bands of constant streamwise-velocity deficit. An associated radius for the bands is calculated by redistributing the area of the bands (in the y, z plane) into annular rings. This provides a radial profile for the strain, similar to a mixing layer. The mixing length l_m is then calculated by integrating the strain profile and dividing it by the maximum strain value $S_{\max}$. With this mixing length, the initial eddy viscosity is computed for the entire flow field based on $\nu_T = 0.01 \times {l_m}^2 \times S$. Here the peak shear stress in a mixing layer is approximated with $0.01 \times \Delta U^2$, where ΔU^2 is the peak velocity difference [21]. This approach assumes that the bulk of the strain is created by the fuselage. This is supported by the observation that the contributions to the total strain away from the fuselage are about one order of magnitude smaller. Atmospheric turbulence and ground effects are not considered.

The initial eddy-viscosity level is a significant parameter when attempting to model the mixing effect of the wake. Thus, the sensitivity to the initial eddy-viscosity level was investigated by varying the level by a factor of 5 (upward and downward). The initial field was subsequently run out to 20 spans behind the tail. Fig. 3 shows the downstream variation of the maximum eddy viscosity in the domain. The case where the baseline ν_T was multiplied by a factor 5 shows a very steep decline in eddy viscosity within the first span. The rapid variation of the eddy viscosity (relative to variations in the mean flow) suggest that the initial eddy viscosity is far from the equilibrium value for this mean flow. The results would, therefore, suggest that the turbulence viscosity was chosen too high for this case. The case where ν_T was 0.2 of the baseline shows less variation with time, but still varies more rapidly than the standard case. The small undulations of ν_T for the nominal initialization value suggests that the eddy viscosity field chosen is a good representation of the 'actual field'.

Fig. 4 shows the vortex trajectories for three turbulent CFD runs in comparison to a laminar case. The tip vortex trajectories show little variation with choice of initial turbulence level. An increase in eddy viscosity leads both to a decrease in the flap vortex strength and to a decrease in the distance between the flap and the tip vortex. These effects are due to increased mixing across the center line as well as changes in the vorticity flux between the vortices. The results for the laminar case are distinctly different with multiple vortices present. Table 1 lists the variation in the tip Γ_T and flap Γ_f vortex circulation, as well as the mid-field separation parameter δ_{yz} measured at $x/b = 10.0$, with the level of the initial eddy viscosity setting. The nondimensional parameter δ_{yz} is defined as d/b_c, where d is the distance between the centroids of the flap and tip vortices and b_c is the centroid distance between the left and right wing total vorticity. There is comparatively little variation in δ_{yz} between the baseline case and a case with a much lower eddy viscosity while the higher initial eddy-viscosity choice produces a much smaller δ_{yz}. The experimentally observed value was 0.81.

A more detailed comparison between laminar and turbulent calculations is given in Fig. 5. This shows vorticity contours and circulation levels at $x/b = 20$ for two calculations starting from the same field at $x/b = 0$. In this case, the laminar calculation shows three vortex pairs persisting to 20 spans. The turbulent calculation shows only two vortex pairs. In the turbulent calculation, there is also a loss of vorticity along the centerline during the early evolution (as discussed in the next section) yielding

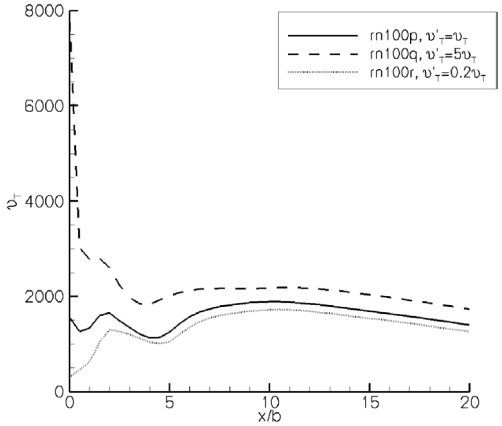

Fig. 3. Variation of maximum eddy viscosity in the field with distance behind the airplane. Comparison between the nominal eddy-viscosity initialization based on the fuselage wake and two arbitrarily altered settings.

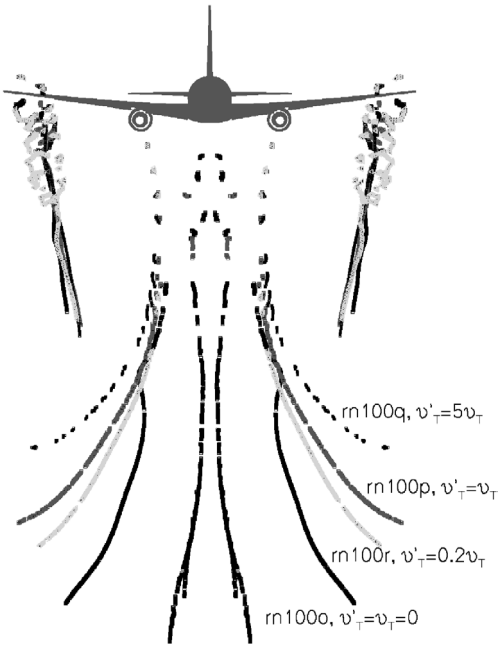

Fig. 4. Vortex core trajectories for a laminar CFD run and three turbulent CFD runs with different initialization levels of the eddy viscosity (up to $x/b = 20.0$). ν_T is the nominal level estimated from the fuselage wake.

Table 1
Summary of downstream wake parameters at $x/b = 10$ with variation in initial eddy viscosity

Case	ν'_T/ν_T	Γ_T	Γ_f	δ_{yz}
rn100p	1.0	0.110	0.032	0.83
rn100q	5.0	0.110	0.027	0.73
rn100r	0.2	0.110	0.031	0.85

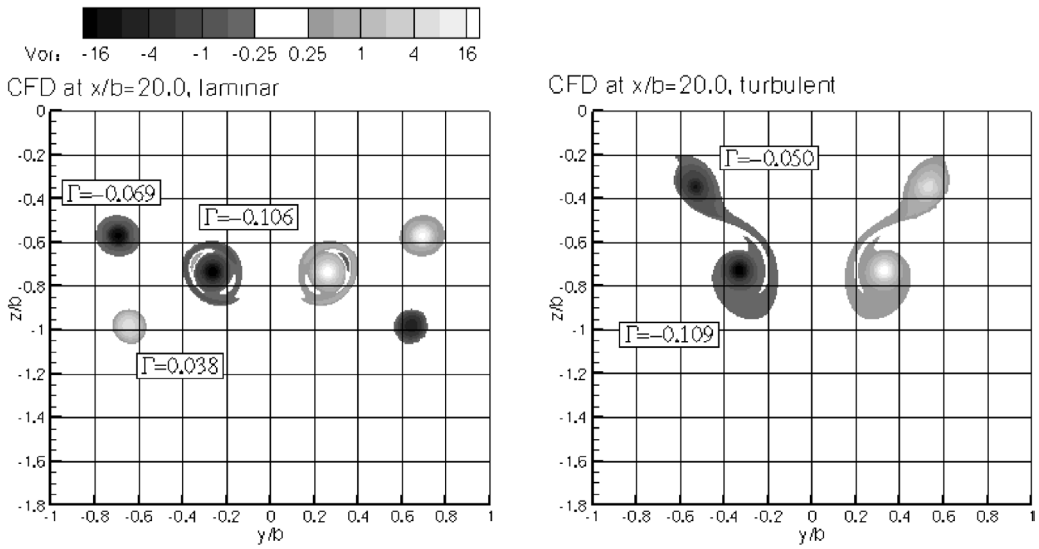

Fig. 5. Comparison of vorticity contours at $x/b = 20.0$ for laminar and turbulent CFD.

different circulation values compared to the laminar run. The above results (in conjunction with Section 3 results) show that the current CFD approach using the SARC turbulence model provides a physically more appropriate approach for predicting near-field trailing vortex flows than a laminar calculation. The comparison also shows the importance of including a fuselage, since the fuselage wake is a key contributor to the turbulent mixing.

The numerical approach was further evaluated on survey data interpolated to three different grids. On the standard grid, a mixing length of $l_m = 0.040$ was obtained with $\delta_{yz} = 0.70$. The coarsest grid with 33 000 points resulted in a strain field with smaller magnitude and yielded a $l_m = 0.024$, with $\delta_{yz} = 0.73$ at $x/b = 10.0$. The solution for a very fine grid of 100 000 points indicated little change from the standard grid with $l_m = 0.042$ and $\delta_{yz} = 0.69$. A robust and grid insensitive numerical approach is obtained with variation of $\delta_{yz} = \pm 0.01$. The standard time step was 0.025 and this showed negligible variation from cases run at smaller time steps of 0.0125.

3. Results

Experimental and computational results are given for a range of airplane-flap configurations; these results show one-pair, two-pair, and three-pair vortex systems downstream of the airplane up to $x/b = 10.0$. The initial results focus on the qualitative description of the near-field dynamics of trailing vortices from airplanes with flaps deployed. This is followed by a quantitative comparison between experimental vorticity field surveys and CFD at two near-field wake locations. Finally, the CFD is used to predict mid-field parameters aimed at assessing potential for vortex breakup. The mid-field parameters are compared to estimated values taken from towing-tank visualizations.

3.1. Qualitative description of near-field dynamics

Fig. 6 shows an experimental vorticity survey measured at the tail of the airplane with flaps deployed (typical of an approach configuration). The lowest contour level of 0.5 is less than 1% of the peak vorticity in the field. Vortices are visible from the tip, the outer edge of the outboard flap, the outer edge of the inboard flap, the side of body and the horizontal tail. The experimental data has been made symmetric and the full domain is shown for clarity. Engine thrust or the presence of a landing gear are not included in the surveys. The position $x = 0$ corresponds to the tail of the airplane, where the CFD is initialized.

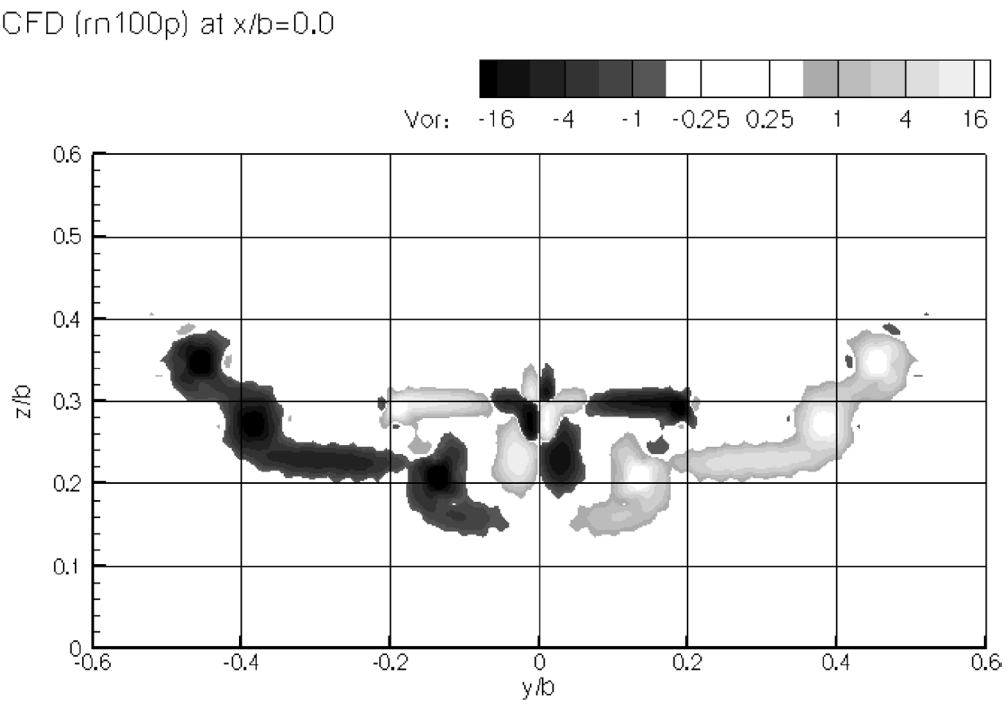

Fig. 6. Wind tunnel survey of vorticity behind an airplane in a typical approach configuration, with flaps down, measured at the tail.

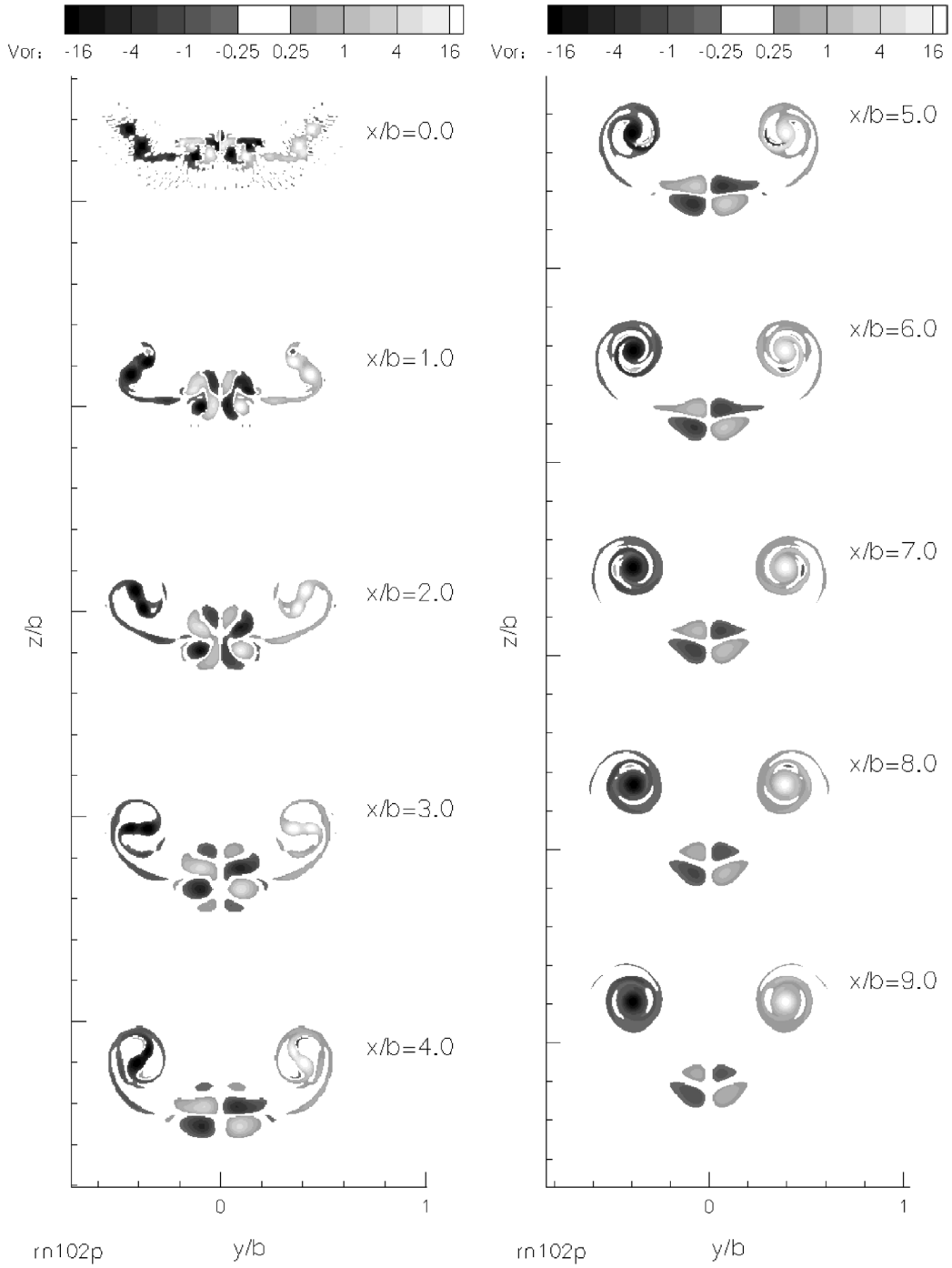

Fig. 7. Snapshots of calculated wake vortex evolution behind an airplane with flaps down (case rn102p). Data at $x/b = 0.0$ from experimental survey.

Fig. 7 shows the evolution of wake vortices behind an aircraft with a spanload typical of an approach configuration. Plotted are vorticity contours from 0 to 9 spans downstream, with an offset applied to the vertical axis and the data mirrored about the center plane for better visualization. Initially, a complex multiple-vortex system is visible. The outboard-flap and wing-tip vortices roll up within five spans into a single distinct vortex later on referred to as the tip vortex. The side of body vortices

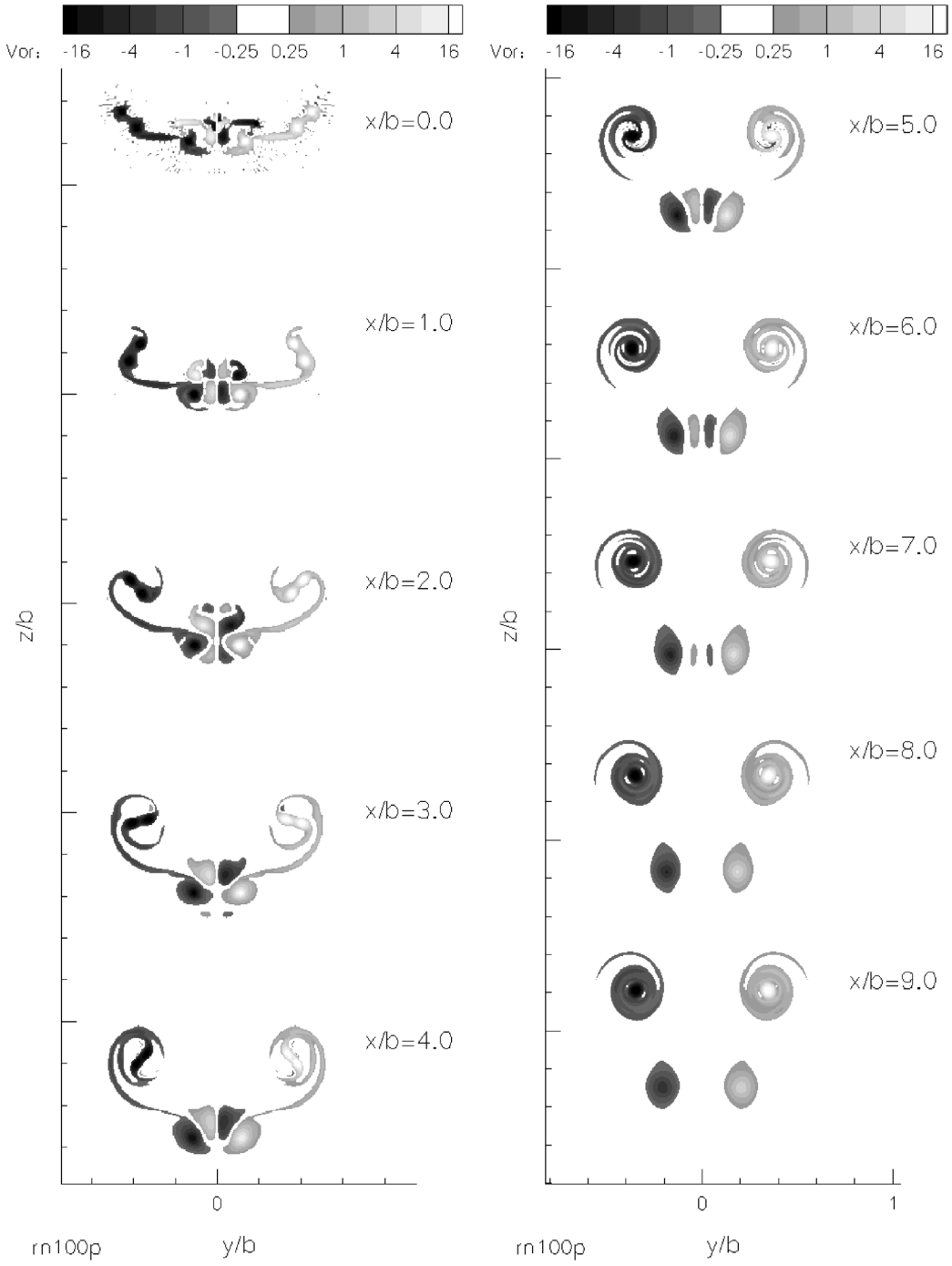

Fig. 8. Snapshots of calculated wake vortex evolution behind an airplane with flaps down (case rn100p) and a slightly stronger initial inboard flap vortex compared to data shown in Fig. 7. Data at $x/b = 0.0$ from experimental survey.

cancel one another out through diffusion across the centerline, and are absent after 3 wing spans. The inboard-flap vortices and the tail vortices descend down together with very little spacing between them. Vorticity cancellation decreases the flap and tail circulation until they disappear just downstream of $x/b = 12.0$. The classification 'one-pair system' is suggested for such a case.

Fig. 8 shows the wake evolution for a different spanload, which is still characteristic of an approach configuration. The tail vortices are positioned between the flap vortices at 5 spans and quickly loose strength marked by their disappearance at

$x/b = 8.0$. The flap vortices are able to preserve circulation as they escape vortex merger and significant centerline diffusion. The flap vortices continue to orbit around the tip vortices and are well preserved at 20 spans resulting in a 'two-pair vortex system'. This classification is limited to the mid-field; far downstream a single vortex pair is expected for all cases. It is worth noting that both cases represent typical approach span and tail loads. Seemingly small changes in the initial vorticity distribution can lead to distinctly different near-field vorticity systems providing a wide range of design space for any proposed active vortex-alleviation system. We also note that thrust effects have so far been neglected. The enhanced mixing due to thrust will undoubtedly effect the multiple-vortex system.

3.2. Comparison between CFD and experiment

Quantitative results are now given for one-, two- and three-pair trailing-vortex systems. These cases were chosen as they are distinctly different in the mid field. In addition, they provide detailed information about the near-field wake evolution for a number of typical approach span loads. A vortex system is referred to as 'one pair' if only the tip vortices are preserved and the flap and tail vortices have essentially disappeared, as shown in Fig. 7. A comparison between the CFD and experiment is given in Fig. 9. The data is plotted with the lowest contour level at 0.25. This shows some noise in the initial field but these low contour levels of vorticity become important further downstream and account for significant parts of the circulation. Flow unsteadiness, vibration of the model, vibration of the 5-hole probe, and processing of the data acquired from the moving probe all contributed to small errors in the measured velocity. However, the error is largely free from bias, so integrated quantities such as vortex circulation and centroid are not particularly sensitive to it.

For the case of Fig. 9, experimental data was only acquired up to $x/b = 5.5$. The plots show the transverse vorticity contours as well as circulation values for the dominant vortices. The agreement with the experimental data is very good in terms of the general position of the vortices. At the same time a comparison between the vortex sheet predicted numerically and obtained experimentally suggests drop outs in the experimental data at the lowest contour levels. This may account for the sometimes lower overall circulations levels relative to the numerical predictions. The tail vortex has almost disappeared at $x/b = 10.0$ and the ratio between flap to tip vortex circulation is less than 6%. Both the tail and flap vortex drop below the 0.25 contour level at $x/b = 12.0$ and this case is called a 'one-pair system'. The differences in the flap-vortex circulation between the CFD and experimental data are not significant since they translate to a small downstream shift in the demise of the vortices.

Fig. 10 gives vorticity contours for a two-pair system of co-rotating vortices where the tail vortex has disappeared by $x/b = 10.0$. The principal difference between this case and Fig. 9 is a change to the inboard flap at the side of body resulting in a stronger flap vortex. The data at $x/b = 5.5$ illustrates very good agreement in the general vorticity field between CFD and experiment. The circulation levels are slightly higher for the computed tail and flap vortices compared to experimental data. However, discontinuities in the experimental data make it difficult to draw clear lines between the flap and tip vortex. The results of Figs. 9 and 10 clearly indicate that small differences in the span or tail-load distribution can lead to a substantially different vortex system within just a few spans behind the tail. The CFD correctly predicts the two-pair system at $x/b = 10.0$ as observed experimentally, with only minor differences in circulation levels.

Fig. 11 shows the near-field evolution of a three-pair vortex system. In this case the tail angle was changed to reduce the strength of the tail vortex, the span of the inboard flap was increased to move the flap vortex outboard, and the aileron was deflected to increase the loading and move the tip vortex outboard. At 5.5 spans the tail vortex centroid is located beneath the flap vortex and further away from the center line compared to the previously discussed cases. The tail vortex escapes cancellation on the centerline and retains significant strength until $x/b = 10.0$. The agreement with experimental data at both survey stations appears excellent. The flap vortex has swung further around the tip vortex when compared to the two-pair case and it maintains significant strength.

3.3. CFD prediction of mid-field parameters

The above comparisons show that the CFD is capable of capturing the dominant mechanisms of the near-field wake evolution. In particular, the CFD captures the merger and demise of different vortices, yielding the key features of the mid-field wake. In order to assess the potential for active vortex control, values for mid-field parameters such as the circulation ratio and the vortex-spacing are required [22]. Table 2 summarizes the CFD predictions for these parameters at $x/b = 10$ for test cases investigated in the 14×22 Wind Tunnel. A comparison between the numerically and experimentally derived values for δ_{yz} show typical agreement to within roughly 10%. The observed differences are likely due to uncertainties in the experimental measurements, such as poor resolution of the lowest vorticity contours, as well as numerical-modeling limitations. Modeling of the turbulence both at the tail with an algebraic model and as it evolves with the SARC model is seen as the most likely source of error. The algebraic model may not give a good enough estimate of the turbulent stresses in the body wake and may underpredict the turbulence levels in the vortex cores. Another potential source for the δ_{yz} discrepancies is the quasi-3D approximation.

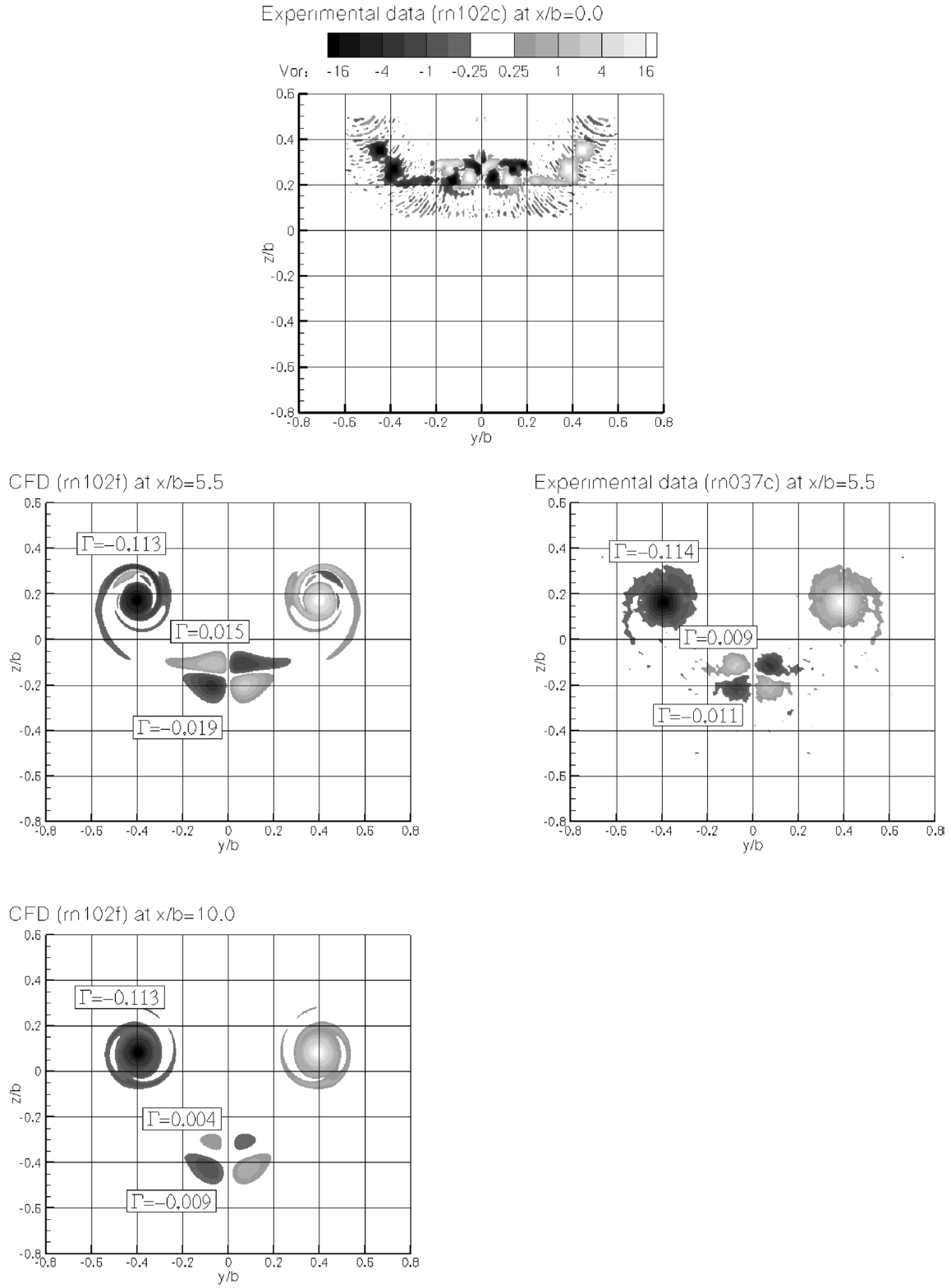

Fig. 9. Near-field wake vortex evolution for a 'one-pair system' at $x/b = 5.5$ and $x/b = 10$ from (a) CFD and (b) experiment (typical approach spanload distribution rn102).

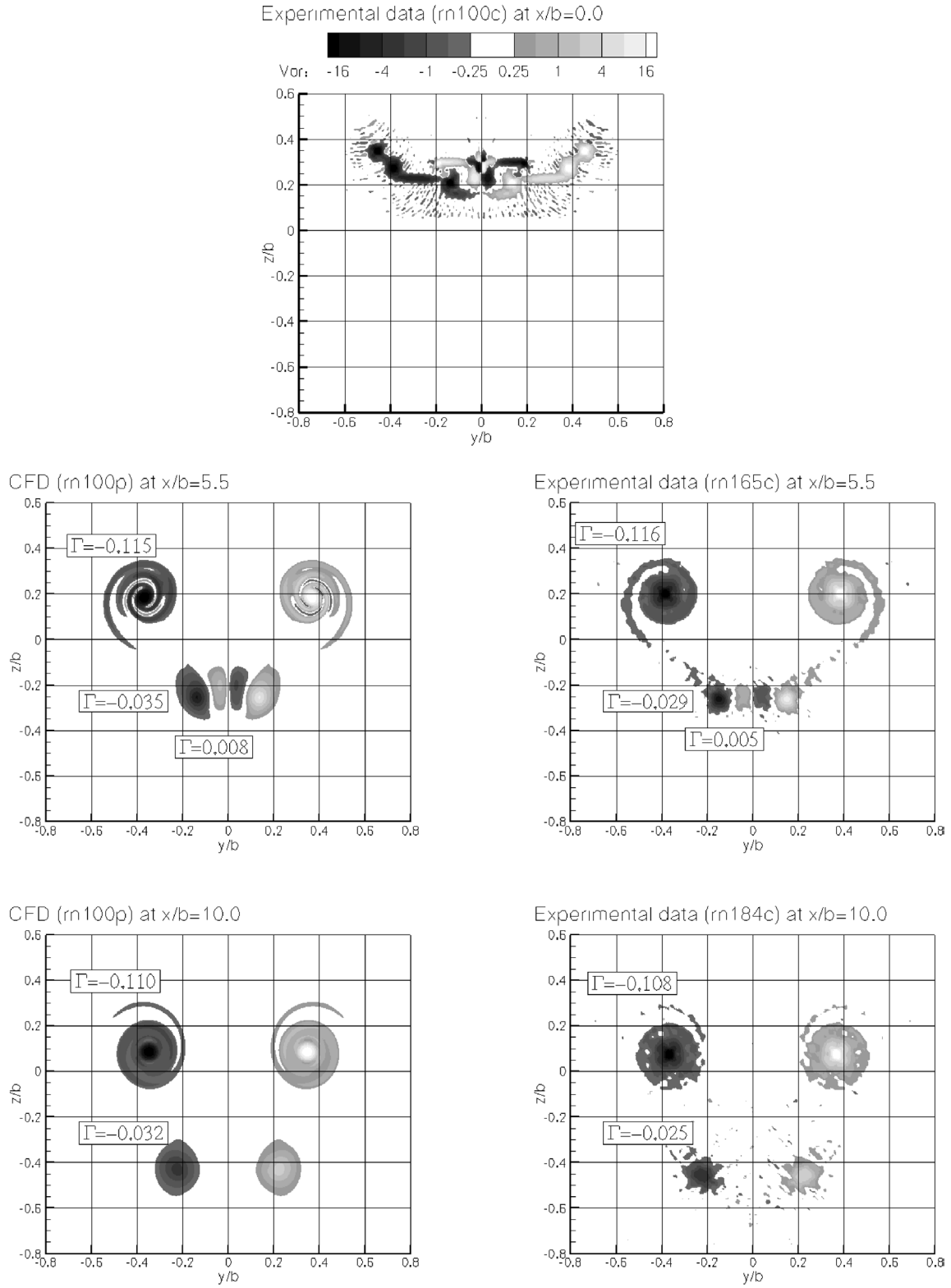

Fig. 10. Near-field wake vortex evolution for a 'two-pair system' at $x/b = 5.5$ and $x/b = 10$ from (a) CFD and (b) experiment (typical approach spanload distribution rn100).

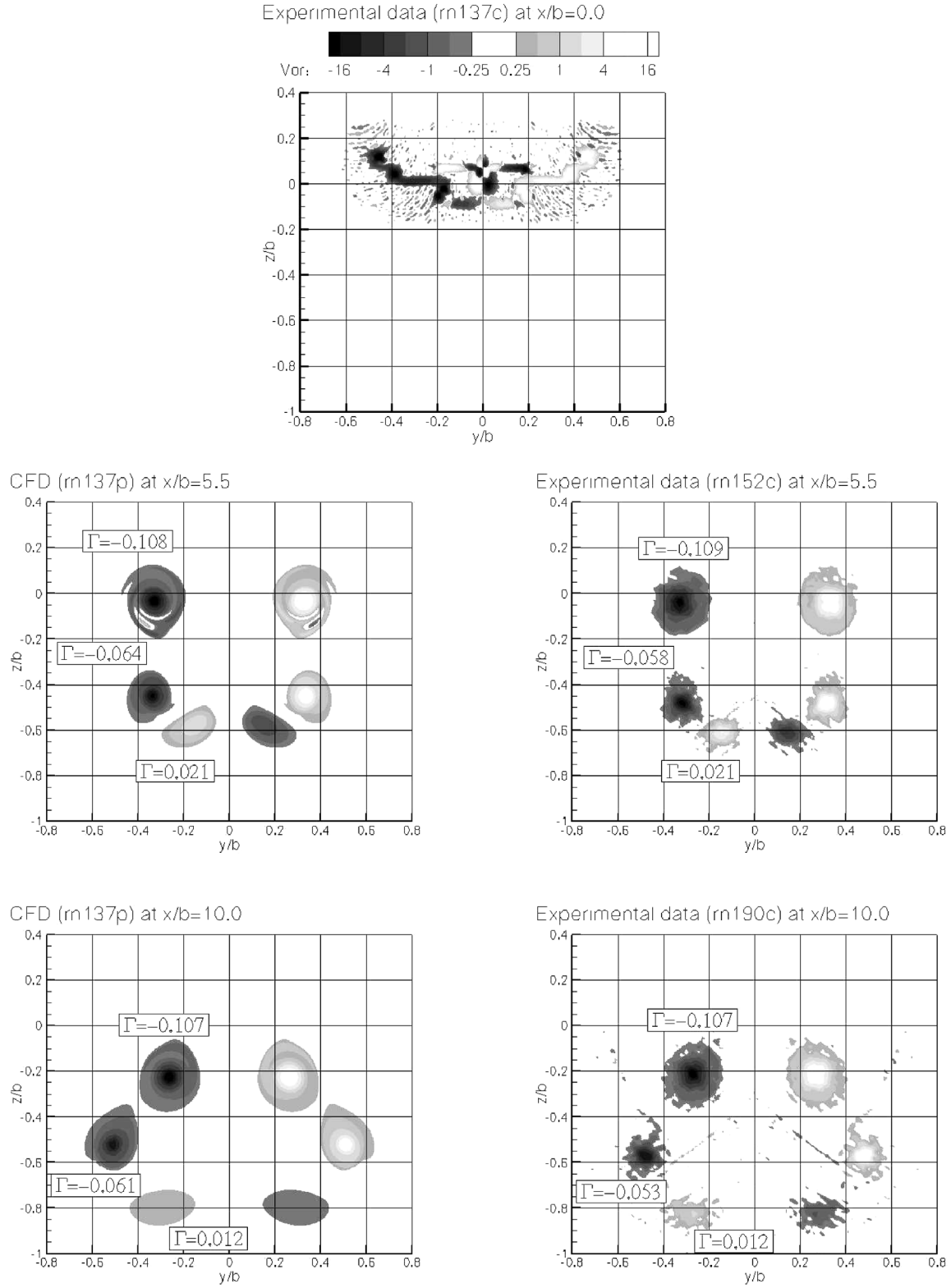

Fig. 11. Near-field wake vortex evolution for a 'three-pair system' at $x/b = 5.5$ and $x/b = 10$ from (a) CFD and (b) experiment (typical approach spanload distribution rn137).

Table 2
Summary of downstream wake parameters at $x/b = 10$

Case	$\frac{\Gamma_f}{\Gamma_T+\Gamma_f}$	δ_{yz}	δ_{yz}, exp	$\Delta\delta_{yz}$
rn100p	0.23	0.83	0.81	2%
rn113p	0.29	0.61[a]	0.67[a]	9%
rn131p	0.23	0.70	0.84	19%
rn137p	0.37	–	–	–
rn138p	0.33	0.65	0.71	9%

[a] Three vortex pairs observed; δ values neglect tail vortices.

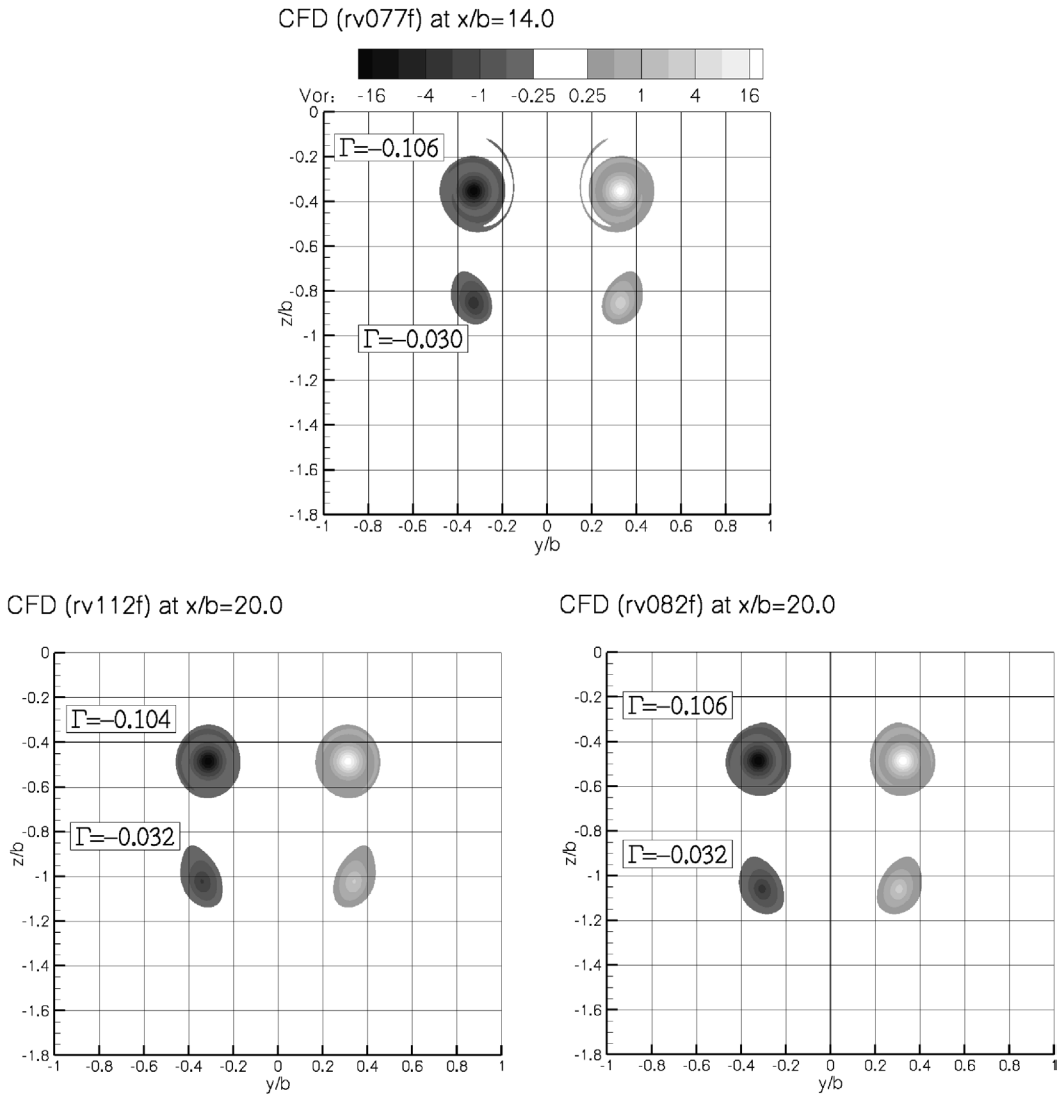

Fig. 12. Vorticity contours where the flap vortex has moved below the tip vortex for three cases with constant wing circulation but different tail circulations.

Since the spacing parameter δ_{yz} changes in time (as the flap vortex orbits the tip vortex), a fixed mid-field measure is needed. We consider the value of δ_{yz} measured when the flap vortex is under the tip vortex and refer to it as $\bar{\delta}_z$. This parameter has the advantage of being measurable using flow visualizations in the towing tank. It has also been shown to correlate with the time required to achieve breakup when using active control [22].

Table 3
Summary of downstream wake parameters at the location where the flap vortex and moved below the tip vortex and $\bar{\delta}_z$ is measured

Case	$\frac{\Gamma_f}{\Gamma_T+\Gamma_f}$	$\bar{\delta}_z$	$\bar{\delta}_z$, exp	$\Delta\bar{\delta}_z$	x/b
rv054f	0.26	0.90	0.77	14%	16.0
rv077f	0.20	0.75	0.68	10%	14.0
rv082f	0.22	0.89	0.93	4%	20.0
rv112f	0.23	0.84	0.76	11%	20.0
rv115f	0.17	0.97	0.85	14%	20.0

Fig. 12 provides a comparison of three test cases with approximately the same wing circulation but differences in tail loadings, with circulations ranging from 15.1 to 22.1 percent of the wing value. The CFD values of $\bar{\delta}_z$ are based on vorticity peak locations. The case with the smallest tail circulation has a nominal tail angle of attack of 2 degrees. A $\bar{\delta}_z$ of 0.75 is found numerically at $x/b = 14.0$, where the inboard vortex has moved below the tip vortex. An experimental value of 0.68 was derived from flow visualization showing reasonable agreement between the CFD and experiment; here the CFD is initialized with survey data from the BVWT. A small increase of tail circulation up to 18.6% of total wing circulation resulted in a rise in $\bar{\delta}_z$ to 0.84 and this is obtained at $x/b = 20.0$. A further increase in tail loading yields $\bar{\delta}_z = 0.89$ at $x/b = 20.0$. These changes in $\bar{\delta}_z$ can also be achieved through wing spanload variations, so there is nothing unique about the tail loading. This variation of the tail load has, therefore, only demonstrated that small alterations of the lift distribution may yield substantially different $\bar{\delta}_z$. This, in turn, can be significant when considering some form of active control. Table 3 provides an overview of results for several cases where both initial surveys and measured $\bar{\delta}_z$ were available. The predicted values for $\bar{\delta}_z$ are within 15% of the experimental values. Slightly higher uncertainties were expected for this test series due to a slightly coarser grid in the wind tunnel wake survey. In addition, the visually derived values for $\bar{\delta}_z$ from the towing tank are based on dye concentration and not on vorticity.

4. Conclusions

The evolution of trailing vortices in the near field of flaps-down airplane configurations has been studied using a combination of experiments and CFD. The experiments included wind-tunnel wake surveys and flow visualizations in a towing tank. The experimental results are used to initialize the CFD calculations, and to validate the CFD for predicting the near-field development. The CFD is based on a quasi-3D approximation to the Reynolds-Averaged Navier–Stokes (RANS) equations. The SA turbulence model is used with rotation and curvature corrections. Initial eddy viscosity levels are calculated based on the strain field associated with the streamwise velocity using an algebraic model. Sensitivity studies show that the turbulence initialization process is robust, yielding small changes in the mid-field wake with modest changes in the initial eddy-viscosity levels. Comparisons with experimental data ten spans downstream of the airplane show that the turbulent approach gives a qualitatively and quantitatively superior estimate of the flow field compared to laminar simulations.

The results show that realistic flaps-down wing and tail loadings can lead to single or multiple vortex pairs ten to twenty spans downstream of the airplane. The inclusion of fuselage-wake turbulent-mixing effects is found to be essential to capturing the correct near-field development. This also implies the importance of including a fuselage if an airplane-like vortex sheet is to be investigated. Results from the experiments and CFD show very-good overall agreement. The CFD properly predicts the number, strength and position of the vortices in the mid field. In the absence of significant turbulence in the wake, vortex interactions are likely to be dominated by instability prior to vortex merger or vortex cancellation. For applications where these effects could be important a higher fidelity CFD approach such as LES may be required.

Earlier studies found that the effectiveness of some active schemes for breaking up the trailing vortices depended on the spacing between co-rotating vortices. Results for the current study show that the RANS-based CFD can be used to predict the spacing parameter, and to assess the potential for vortex breakup. This approach also has the advantage of allowing for the use of conventional high-lift models for judging wake-control schemes, since wind-tunnel wake surveys at far-downstream locations are not required. Conventional high-lift models can be used to study the effects of landing gear, flap geometry, and control-surface deflections.

The CFD approach also offers the ability to study thrust effects, which are generally neglected in wind-tunnel testing. Current efforts are aimed at coupling the jet plume into the wake-vortex calculation. This will provide a more realistic picture of the near-wake evolution in flight conditions. This capability can also be used to study the entrainment of jet plumes at cruise conditions. The plume/wake interactions can have an influence on the long-term persistence of contrails under some flight conditions.

References

[1] T. Quackenbush, A. Bilanin, P. Batcho, R. McKilipp, B. Carpenter, Implementation of vortex wake control using SMA-actuated devices, in: Proc. SPIE, vol. 3044, 1997, pp. 134–146.
[2] S.C. Rennich, S.K. Lele, A method for accelerating the destruction of aircraft wake vortices, J. Aircraft 36 (1999) 398–404.
[3] D. Fabre, L. Jacquin, Stability of a four-vortex aircraft wake model, Phys. Fluids 12 (2000) 2438–2443.
[4] J. Ortega, Ö. Savaş, Rapidly growing instability mode in trailing multiple-vortex wakes, AIAA J. 39 (2001) 750–754.
[5] J.D. Crouch, G.D. Miller, P.R. Spalart, Active-control system for breakup of airplane trailing vortices, AIAA J. 39 (2001) 2374–2381.
[6] St. Fell, R. Staufenbiel, Formation and structure of vortex systems generated by unflapped and flapped wing configurations, Z. Flugwiss. Weltraumforsch 19 (1995) 366–379.
[7] A.C. de Bruin, S.H. Hegen, P.B. Rohne, P.R. Spalart, Flow field survey in the trailing vortex system behind a civil aircraft model at high lift, AGARD-CP-584, 1996, pp. 25-1–25-12.
[8] L. Jacquin, D. Fabre, P. Geffroy, E. Coustols, The properties of a transport aircraft wake in the extended near-field: an experimental study, AIAA Paper No. 2001-1038, 2001.
[9] C. Bellastrada, C. Breitsamter, B. Laschka, Investigation of turbulent wake vortex originating from a large transport aircraft in landing configuration, in: Proc. CEAS Aerospace Aerodynamics Research Conference, 2002, pp. 31.1–31.10.
[10] J.D. Jacob, Ö. Savaş, Vortex dynamics in trailing wakes of flapped rectangular wings, AIAA Paper No. 97-0048, 1997.
[11] R. Stuff, The near-far field relationship of vortices shed from transport aircraft, AIAA Paper No. 2001-2429, 2001.
[12] D.A. Durston, S.M. Walker, D.M. Driver, S.C. Smith, Ö. Savaş, Wake vortex alleviation flow field studies, AIAA Paper No. 2004-1073, 2004.
[13] E. Coustols, E. Stumpf, L. Jacquin, F. Moens, H. Vollmers, T. Gerz, Minimized wake: a collaborative research programme on aircraft wake vortices, AIAA Paper No. 2003-0938, 2003.
[14] A. Benkenida, G. Jonville, D. Darracq, Numerical study of wake vortices of generic aircraft model, AIAA Paper No. 2001-2428, 2001.
[15] E. Stumpf, Numerical study of four-vortex aircraft wakes and layout of corresponding high-lift configurations, AIAA Paper No. 2004-1067, 2004.
[16] M. Shur, M. Strelets, A. Travin, P. Spalart, Two numerical studies of trailing vortices, AIAA Paper No. 98-0595, 1998.
[17] P. Spalart, S.R. Allmaras, A one-equation turbulence model for aerodynamic flows, AIAA Paper No. 92-0439, 1992.
[18] M.L. Shur, P. Spalart, On the sensitization of turbulence models to rotation and curvature, Aerospace Sci. Technol., 1997.
[19] J.P. Crowder, R.L. Watzlavick, T.K. Krutckoff, Airplane flow-field measurements, in: AIAA/SAE World Aviation Congress, vol. 8 (975535), 1997, pp. 1–9.
[20] S.E. Rogers, D. Kwak, An upwind differencing scheme for the time-accurate incompressible Navier–Stokes equations, AIAA Paper No. 88-2583-CP, 1988.
[21] A.A. Townsend, The Structure of Turbulent Shear Flow, Cambridge University Press, New York, 1976.
[22] J.D. Crouch, G.D. Miller, P.R. Spalart, Simplified modeling for flaps-down airplane trailing vortices, Bull. Am. Phys. Soc. 46 (2001) 159.